NBSIR 82-2572

Status of Electron Transport Cross Sections

U.S. DEPARTMENT OF COMMERCE
National Bureau of Standards
Washington, DC 20234

September 1982

Prepared for:
Office of Naval Research
Arlington, Virginia 22217

Space Science Data Center
NASA Goddard Space Flight Center
Greenbelt, Maryland 20771

Office of Health and Environmental Research
Department of Energy
Washington, DC 20545

NBSIR 82-2572

STATUS OF ELECTRON TRANSPORT CROSS SECTIONS

S. M. Seltzer and M. J. Berger

U.S. DEPARTMENT OF COMMERCE
National Bureau of Standards
Washington, DC 20234

September 1982

Prepared for:
Office of Naval Research
Arlington, Virginia 22217

Space Science Data Center
NASA Goddard Space Flight Center
Greenbelt, Maryland 20771

Office of Health and Environmental Research
Department of Energy
Washington, DC 20545

U.S. DEPARTMENT OF COMMERCE, Malcolm Baldrige, *Secretary*
NATIONAL BUREAU OF STANDARDS, Ernest Ambler, *Director*

Status of Electron Transport Cross Sections*†

Stephen M. Seltzer and Martin J. Berger
National Bureau of Standards
Washington, D.C. 20234

This report describes recent developments and improvements pertaining to cross sections for electron-photon transport calculations. The topics discussed include: (1) electron stopping power (mean excitation energies, density-effect correction); (2) bremsstrahlung production by electrons (radiative stopping power, spectrum of emitted photons); (3) elastic scattering of electrons by atoms; (4) electron-impact ionization of atoms.

Key words: bremsstrahlung; cross sections; elastic scattering; electron-impact ionization; electrons; photons; stopping power; transport.

---

*Summary of a paper presented at the Annual Meeting of the American Nuclear Society, June 7-11, 1982, Los Angeles, California.

†This work was supported by the Office of Naval Research, by the National Space Science Data Center at the NASA Goddard Space Flight Center, and by the Office of Health and Environmental Research of the Department of Energy.

Status of Electron Transport Cross Sections*†

Stephen M. Seltzer and Martin J. Berger
National Bureau of Standards
Washington, D.C. 20234

This report describes recent developments and improvements pertaining to cross sections for electron-photon transport calculations. The topics discussed include: (1) electron stopping power (mean excitation energies, density-effect correction); (2) bremsstrahlung production by electrons (radiative stopping power, spectrum of emitted photons); (3) elastic scattering of electrons by atoms; (4) electron-impact ionization of atoms.

Key words: bremsstrahlung; cross sections; elastic scattering; electron-impact ionization; electrons; photons; stopping power; transport.

---

*Summary of a paper presented at the Annual Meeting of the American Nuclear Society, June 7-11, 1982, Los Angeles, California.

†This work was supported by the Office of Naval Research, by the National Space Science Data Center at the NASA Goddard Space Flight Center, and by the Office of Health and Environmental Research of the Department of Energy.

1. INTRODUCTION

In this paper we highlight certain improvements to the cross-section data base for various Monte Carlo computer codes such as ETRAN [1],[1] EGS [2], SANDYL [3], TIGER [4], ACCEPT [5], etc., which are used to calculate the transport of electrons and associated bremsstrahlung at energies from ~ 10 keV up to 1 GeV. The discussion will be in terms of the cross-section information needed by the ETRAN code [1], as supplied by the program DATAPAC [6], but is also applicable to the SANDYL, TIGER, and ACCEPT codes which are decendants of ETRAN.

2. ELECTRON STOPPING POWER

2.1. Mean excitation energies

We have completed a critical review of the mean excitation energy I, the key quantity in the Bethe theory of the collision stopping power. Based on current information derived from stopping-power and range data, oscillator-strength distributions for gases, and dielectric-response functions for condensed media, I-values were selected for 43 elemental substances and 54 compounds. I-values for other elements were obtained by interpolation with respect to atomic number (see table 1 and fig. 1). I-values for other compounds were obtained through the application of the Bragg additivity rule, using I-values for atomic constituents modified to take into account chemical binding and phase effects (see table 2). Further details can be found in references [7-9].

2.2. Density-effect correction

The density-effect correction, the other non-trivial quantity entering into the Bethe formula, was also re-examined. For this correction, DATAPAC uses the algorithm of Sternheimer and Peierls [10], which is a universal fit to previously calculated results. The use of this fit involves some sacrifice in accuracy, and in recent work [9,11] we have gone back to the numerical evaluation of the density effect using Sternheimer's [12] model in conjunction with updated values of mean excitation energies and atomic binding energies. We have found that our numerical results for the density effect are in good agreement with those calculated by Inokuti and Smith [13] for aluminum and by Ashley [14] for water with semi-empirical dielectric-response functions. The changes in the collision stopping power that result from using the new numerical results instead of the Sternheimer-Peierls algorithm are shown in figure 2 for selected materials.

---

[1]Numbers in brackets indicate the literature references at the end of this paper.

2.3. Conclusions

(i) The analysis of experimental data confirms the theoretical prediction [15] that, due to atomic shell effects, I/Z is an irregular function of Z. (ii) The Bragg additivity rule, with a simple assignment of I-values for atomic constituents that takes into account chemical binding and phase effects, provides an accurate representation of the I-values for over 50 compounds and is expected to be a reliable method for predicting I-values for other materials. (iii) The combined effect of using the new I-values and density-effect corrections results in changes of no more than 3-4%, more typically 1-2%, in the collision stopping power as compared to our older values from DATAPAC.

3. BREMSSTRAHLUNG PRODUCTION BY ELECTRONS

3.1. Radiation stopping power

As discussed in reference [16], DATAPAC makes use of a combination of Bethe-Heitler Born-approximation formulas, with empirical corrections, at energies below 50 MeV, and above 50 MeV uses the exact high-energy theory of Davies, Bethe, Maximon, and Olsen [17], which includes a Coulomb correction. A significant improvement in the calculation of the cross section for bremsstrahlung in the field of the screened nucleus was made by Pratt *et al.* [18], who solved the Dirac equation numerically for a static, screened Coulomb potential, and evaluated the bremsstrahlung matrix elements numerically from the wave functions. These authors give the cross section, differential in emitted photon energy, for atomic numbers Z from 2 to 92 and for electron kinetic energies from 1 keV to 2 MeV.

For the calculation of electron radiative stopping powers [9,19], we have bridged the gap between 2 and 50 MeV by interpolating between the results of Pratt *et al.* and the results from the high-energy theory. Two additional improvements were also made: (a) the high-energy results were re-evaluated using screening functions based on Hartree-Fock rather than Thomas-Fermi form factors; (b) the contribution from bremsstrahlung produced in the field of the atomic electrons was evaluated on the basis of Haug's [20] cross section. The results can be conveniently summarized in terms of the scaled radiative energy-loss functions

$$\phi_{rad}^{(n)}(T) = \frac{1}{\alpha r_e^2}\,\frac{1}{T+mc^2}\int_0^T \frac{k}{Z^2}\,\frac{d\sigma^{(n)}(k,T)}{dk}\,dk \quad \text{(electron-nucleus)}$$

and

$$\phi_{rad}^{(e)}(T) = \frac{1}{\alpha r_e^2} \frac{1}{T+mc^2} \int_o^{T'} \frac{k}{Z} \frac{d\sigma^{(e)}(d,T)}{dk} dk \quad \text{(electron-electron)} \ ,$$

where α is the fine structure constant (1/137.03604), r_e is the classical electron radius (2.817938×10^{-13}cm), mc^2 is the electron rest mass (0.5110034 MeV), Z is the atomic number, T is the electron kinetic energy, $\frac{d\sigma}{dk}$ is the bremsstrahlung production cross section differential in emitted photon energy k, either in the field of the atomic nucleus (denoted by superscript n) or in the field of the atomic electrons (denoted by superscript e), and $T' = mc^2T/[T + 2mc^2 - (T(T + 2mc^2))^{\frac{1}{2}}]$ is the maximum possible energy of photons emitted in an electron-electron collision. The radiative stopping power can then be written as

$$\frac{1}{\rho}\left(\frac{dE}{dx}\right)_{rad} = \frac{N_a}{A} \alpha r_e^2 (T+mc^2)\, Z^2 \phi_{rad}^{(n)}(T) \left[1 + \frac{1}{Z} \frac{\phi_{rad}^{(e)}(T)}{\phi_{rad}^{(n)}(T)}\right] \ ,$$

where N_a is Avagadro's number (6.022045×10^{23} mol^{-1}) and A is the atomic weight of the material. Figure 3 gives results for $\phi_{rad}^{(n)}$ from 1 keV to 10 GeV in selected materials. The ratio $\phi_{rad}^{(e)}(T)/\phi_{rad}^{(n)}(T)$, previously assumed equal to unity in DATAPAC, is shown in figure 4 for hydrogen, carbon, and gold. At high energies, this ratio is greater than unity due to the differences in screening and Coulomb effects between the electron-electron and the electron-nucleus systems. At low energies, the ratio tends to vanish due to the lack of a dipole moment for the electron-electron system.

3.2. Spectrum of emitted photons

A similar synthesis for the cross section differential in emitted photon energy is in progress. A further refinement is included to account for the non-zero value of the electron-nucleus cross section at the high-frequency limit (tip of the bremsstrahlung spectrum, k = T). This is accomplished (a) by interpolating between the tip values predicted by Jabbur and Pratt [21] for extremely high energies and those given by Pratt *et al.* [18] for energies below 2 MeV, as illustrated in figure 5; and (b) by applying a Coulomb correction, shown in figure 6, which combines the results of Davies, Bethe, Maximon, and Olsen [17] with the Elwert [22] factor so as to insure that the cross section goes smoothly into the tip value. Figures 7a and b give the cross sections at 50 MeV for carbon and gold, and are typical of the high-energy ($T \geqslant 50$ MeV) results; figures 7c and d, for carbon and gold at 50 keV, illustrate the results for $T \leqslant 2$ MeV. The accuracy of the interpolated results in

the gap region from 2 to 50 MeV is confirmed by the comparisons, shown in figures 8a and b, with the results available from the exploratory, exact numerical calculations of Tseng and Pratt [23], for Aℓ and U at 5 and 10 MeV.

3.3. Conclusions

The use of the cross sections of Pratt *et al.*, together with interpolation linking the low- and high-energy theories, results in a significant improvement over the cross-section package and empirical correction factors used in DATAPAC. The procedures outlined above will provide the basis for a planned comprehensive tabulation of bremsstrahlung cross sections for electron energies greater than 2 MeV.

4. ELECTRON ELASTIC SCATTERING

4.1. Discussion of cross sections

The accurate evaluation of the elastic scattering cross section requires - in principle - exact phase shift calculations for the solution of the Dirac equation for the electron in a screened Coulomb potential. In practice, an approximation is - in most cases - quite adequate in which the cross section is calculated as the product of two factors: (a) the unscreened Mott [24] cross section which includes spin and relativistic effects; and (b) a screening correction term.

We have considered two methods of calculating the screening factor. The first method, introduced by Spencer [25] and used in DATAPAC, consists of using the factor $(1 - \cos\theta)^2/(1 - \cos\theta + 2\eta)^2$ where η is an energy- and Z-dependent screening parameter derived by Molière [26] in a calculation for the Thomas-Fermi atom. The second method consists of using the impulse approximation in which the screening factor is taken to be $[1 - F(q,Z)]^2$, where $F(q,Z)$ is a Hartree-Fock atomic form factor for momentum transfer q and atomic number Z.

At low energies the factorization of the elastic scattering cross section becomes inaccurate (see, *e.g.*, Zeitler and Olsen [27]), and it becomes necessary to carry out a full phase-shift analysis. The most comprehensive calculations of this kind are those of Riley *et al.* [28], who give results at 9 energies from 1 to 256 keV and for selected elements from $Z = 2$ to 92, and who also give a convenient approximation for $Z = 1 - 94$ which facilitates the incorporation of their cross sections into DATAPAC (see also Haggmark *et al.* [29]).

We have investigated the validity of the factorization in terms of the transport (or momentum transfer) cross section $\sigma_1 = \sigma(1 - \overline{\cos\theta})$, where σ is the total cross section (integrated over all angles) and $\overline{\cos\theta}$ is the mean cosine of the scattering angle. As pointed out by Molière [26] and by Bethe [30], the transport cross section

has the dominant influence on the multiple elastic scattering process. In figure 9 we compare the transport cross sections of Riley *et al.* with those from the Molière-Mott approximation and those from the impulse approximation.

4.2. Conclusions

(i) Comparisons with the exact results of Riley *et al.* indicate that the Molière-Mott approximation used in DATAPAC begins to break down, in terms of the transport cross section, at electron energies below ~ 128 keV in Au, ~ 64 keV in Cu, ~ 16 keV in Aℓ, and ~ 4 keV in Be. (ii) To the extent that transport calculations depend only on the transport cross section, the data of Riley *et al.* and/or the results from the Molière-Mott approximation provide sufficient data at all energies. However, it would be desirable to extend the exact calculations to energies somewhat higher than 256 keV for the high-Z elements. (iii) The incorporation of the exact cross sections into the multiple scattering algorithm in DATAPAC could be greatly simplified by retaining the Molière-Mott approximation, but adjusting the screening parameter η so as to obtain the correct value of the transport cross section σ_1. The accuracy of this approximation remains to be investigated.

5. ELECTRON-IMPACT IONIZATION

5.1. Discussion of cross sections

As an energy-loss mechanism, this process is included in the collision stopping power. Knowledge of ionization cross section is needed when including in a transport calculation the emission of x rays subsequent to ionizations of inner shells. Numerous calculations of this cross section, done in various approximations, have been reported. In DATAPAC, we have used the approximate formula of Kolbenstvedt [31] for K-shell ionization, which was derived by the Weizsäcker-Williams method. Recently, the *ab initio* calculations of Scofield [32] have become available for the K and L shells, for $Z \geq 18$, and for $T \geq 50$ keV. We have applied the Weizsäcker-Williams method for all shells, going beyond Kolbenstvedt through the use of more detailed theoretical and experimental photoionization cross sections for soft collisions and through the use of binary-encounter theory for hard collisions. In figures 10 and 11 we compare results from Scofield and from our Weizsäcker-Williams calculations with experimental data [33-51] for Au, Ni, and Aℓ.

5.2. Conclusions

(i) The results obtained by our application of the Weizsäcker-Williams method agree quite well with experiment and with Scofield's rigorous results at energies above about 20 times the ionization threshold energy. (ii) At energies below ~ 20 times the ionization threshold energy, the Weizsäcker-Williams results appear to be more consistent with experimental data than Scofield's results. (iii) The Weizsäcker-Williams method, which requires a modest computational effort, can be used to extend coverage to any energy, atom, and shell of interest (for example, for $Z < 18$ not covered by Scofield). It is a useful alternative to semi-empirical methods for estimating the electron-impact ionization cross section, such as the formula of Lotz [52].

REFERENCES

[1] M. J. Berger and S. M. Seltzer, National Bureau of Standards Report 9837 (1968); see also Oak Ridge National Laboratory Publ. ORNL-RSIC Report CCC-107 (1968).

[2] R. L. Ford and W. R. Nelson, Stanford Linear Accelerator Center Report SLAC-210, UC-32 (1978).

[3] H. M. Colbert, Sandia Laboratories Report SLL-74-0012 (1973).

[4] J. A. Halbleib and W. H. Vandevender, Sandia Laboratories Report SLA-73-1026 (1974).

[5] J. A. Halbleib, Sandia Laboratories Report SAND79-0415 (1979).

[6] M. J. Berger and S. M. Seltzer, National Bureau of Standards Report 9836 (1968); also Oak Ridge National Laboratory Publ. ORNL-RSIC Report CCC-107 (1968).

[7] S. M. Seltzer and M. J. Berger, Intl. J. of Applied Radiation and Isotopes, in press.

[8] M. J. Berger and S. M. Seltzer, Proc. of the Seminar on Charge States and Dynamic Screening of Swift Ions in Solids, Honolulu, Hawaii, Jan. 25-29 (1982), to be published.

[9] M. J. Berger and S. M. Seltzer, National Bureau of Standards Report NBSIR 82-2550 (1982).

[10] R. M. Sternheimer and R. F. Peierls, Phys. Rev. B 3, 3681 (1971).

[11] R. M. Sternheimer, S. M. Seltzer, and M. J. Berger, submitted to Phys. Rev.

[12] R. M. Sternheimer, Phys. Rev. 88, 851 (1952).

[13] M. Inokuti and D. Y. Smith, Phys. Rev. B 25, 61 (1982).

[14] J. C. Ashley, Rad. Res. 89, 32 (1982).

[15] W. K. Chu and D. Powers, Phys. Lett. 40A, 23 (1972).

[16] M. J. Berger and S. M. Seltzer, Phys. Rev. C 2, 621 (1970).

[17] H. Davies, H. A. Bethe and L. C. Maximon, Phys. Rev. 93, 788 (1954); H. Olsen, Phys. Rev. 99, 1335 (1955).

[18] R. H. Pratt, H. K. Tseng, C. M. Lee, L. Kissel, C. MacCallum, and M. Riley, Atomic Data and Nuclear Data Tables 20, 175 (1977); errata in 26, 477 (1981); see also revised data in L. Kissel, C. MacCallum, and R. H. Pratt, Sandia National Laboratories Report SAND81-1337 (1981).

[19] S. M. Seltzer and M. J. Berger, Intl. J. of Applied Radiation and Isotopes, in press.

[20] E. Haug, Z. f. Naturforsch. 30a, 1099 (1975).

[21] R. J. Jabbur and R. H. Pratt, Phys. Rev. 129, 184 (1963); Phys. Rev. 133, B1090 (1964).

[22] G. Elwert, Ann. Physik. 34, 178 (1939).

[23] H. K. Tseng and R. H. Pratt, Phys. Rev. A 19, 1525 (1979).

[24] N. F. Mott and H. S. W. Massey, The Theory of Atomic Collisions (Oxford University Press, London), 2nd edition (1949).

[25] L. V. Spencer, National Bureau of Standards Monograph 1 (1959).

[26] G. Molière, Z. Naturforsch. 3a, 78 (1948).

[27] E. Zeitler and H. Olsen, Phys. Rev. 136, A1546 (1964).

[28] M. E. Riley, C. J. MacCallum, and F. Biggs, Atomic Data and Nuclear Data Tables 15, 443 (1975).

[29] L. G. Haggmark, C. J. McCallum, and M. E. Riley, Trans. Am. Nucl. Soc. 19, 471 (1974).

[30] H. A. Bethe, Phys. Rev. 89, 1256 (1953).

[31] H. Kolbenstvedt, J. Appl. Phys. 38, 4785 (1967).

[32] J. H. Scofield, Phys. Rev. A 18, 963 (1978).

[33] L. M. Middleman, R. L. Ford, and R. Hofstader, Phys. Rev. A 2, 1429 (1970).

[34] K. Ishii, M. Kamiya, K. Sera, S. Morita, H. Tawara, M. Oyamada, and T. C. Chu, Phys. Rev. A 15, 906 (1977).

[35] H. H. Hoffmann, H. Genz, W. Löw, and A. Richter, Phys. Lett. 65A, 304 (1978).

[36] G. R. Dangerfield and B. M. Spicer, J. Phys. B 8, 1744 (1975).

[37] K. H. Berkner, S. N. Kaplan, and R. V. Pyle, Bull. Am. Phys. Soc. 15, 786 (1970).

[38] D. H. Rester and W. E. Dance, Phys. Rev. 152, 1 (1966).

[39] H. Hansen and A. Flammersfeld, Nucl. Phys. 79, 135 (1966).

[40] J. W. Motz and R. C. Placious, Phys. Rev. 136, A662 (1964).

[41] D. V. Davis, V. D. Mistry, and C. A. Quarles, Phys. Lett. 35A, 169 (1972).

[42] S. I. Salem and L. D. Moreland, Phys. Lett. 37A, 161 (1971).

[43] M. Green, Ph.D. Dissertation, Univ. of Cambridge, Cambridge, England (1962); data obtained from reference 42.

[44] Y. K. Park, M. T. Smith, and W. Scholz, Phys. Rev. A 12, 1358 (1975).

[45] W. Hink and A. Ziegler, Z. Physik 226, 222 (1969).

[46] H. Genz, C. Brendel, P. Eschwey, U. Kuhn, W. Löw, A. Richter, P. Seserko, and R. Sauerwein, Institute für Kernphysik, Technische Hochschule Darmstadt, Report IKDA 81/16 (August, 1981).

[47] A. Li-Scholz, R. Collé, I. L. Preiss, and W. Scholz, Phys. Rev. A 7, 1957 (1973).

[48] S. A. H. Seif el Nasr, D. Berényi, and Gy. Bibok, Z. Physik 267, 169 (1974).

[49] L. T. Pockman, D. L. Webster, P. Kirkpatrick, and K. Harwort, Phys. Rev. 71, 330 (1947).

[50] A. E. Smick and P. Kirkpatrick, Phys. Rev. 67, 153 (1945).

[51] J. Jessenberger and W. Hink, Z. Physik A 275, 331 (1975).

[52] W. Lotz, Z. Physik 232, 101 (1970).

[53] N. E. Holden, Pure and Appl. Chem. 51, 405 (1979).

[54] J. F. Ziegler, Handbook of Stopping Cross Sections for Energetic Ions in all Elements, Vol. 5, Pergamon Press, New York (1980).

[55] J. H. Hubbell, W. J. Veigele, E. A. Briggs, R. T. Brown, D. T. Cromer, and R. J. Howerton, J. Phys. Chem. Ref. Data 4, 471 (1975); errata in 6, 615 (1977).

[56] J. H. Hubbell and I. J. Øverbø, J. Phys. Chem. Ref. Data 8, 69 (1979).

[57] J. A. Wheeler and W. E. Lamb, Phys. Rev. 55, 858 (1939); errata in 101, 1836 (1956).

Table 1. Values of the mean excitation energy I for the elements. Unless noted otherwise, the values are for the substance in the condensed phase.

Z	Element	Symbol	A,[a] g/mol	I,[b] eV
1	hydrogen	H	1.0079	19.2 ± 0.4 molecular gas 21.8 ± 1.6 liquid
2	helium	He	4.00260	41.8 ± 0.8 gas
3	lithium	Li	6.941	40 ± 5
4	beryllium	Be	9.01218	63.7 ± 3.0
5	boron	B	10.81	76.0 ± 8.0
6	carbon	C	12.011	78.0 ± 7.0 graphite
7	nitrogen	N	14.0067	82.0 ± 2.0 molecular gas
8	oxygen	O	15.9994	95.0 ± 2.0 molecular gas
9	fluorine	F	18.998403	(115 ± 10) gas
10	neon	Ne	20.179	137 ± 4 gas
11	sodium	Na	22.98977	(149 ± 10)
12	magnesium	Mg	24.305	(156 ± 10)
13	aluminum	Aℓ	26.98154	166 ± 2
14	silicon	Si	28.0855	173 ± 3
15	phosphorus	P	30.97376	(173 ± 15)
16	sulfur	S	32.06	(180 ± 15)
17	chlorine	Cℓ	35.453	(174 ± 15) gas
18	argon	Ar	39.948	188 ± 10 gas
19	potassium	K	39.0983	(190 ± 15)
20	calcium	Ca	40.08	191 ± 8
21	scandium	Sc	44.9559	216 ± 8
22	titanium	Ti	47.88	233 ± 5
23	vanadium	V	50.9415	245 ± 7
24	chromium	Cr	51.996	257 ± 10
25	manganese	Mn	54.9380	272 ± 10
26	iron	Fe	55.847	286 ± 9
27	cobalt	Co	58.9332	297 ± 9
28	nickel	Ni	58.69	311 ± 10
29	copper	Cu	63.546	322 ± 10
30	zinc	Zn	65.38	330 ± 10
31	gallium	Ga	69.72	(334 ± 20)
32	germanium	Ge	72.59	350 ± 11
33	arsenic	As	74.9216	(347 ± 25)

Z	Element	Symbol	A,[a] g/mol	I,[b] eV
34	selenium	Se	78.96	(348 ± 30)
35	bromine	Br	79.904	(343 ± 30) gas (357 ± 30) condensed
36	krypton	Kr	83.80	352 ± 25 gas
37	rubidium	Rb	85.4678	(363 ± 30)
38	strontium	Sr	87.62	(366 ± 30)
39	yttrium	Y	88.9059	(379 ± 30)
40	zirconium	Zr	91.22	393 ± 15
41	niobium	Nb	92.9064	417 ± 15
42	molybdenum	Mo	95.94	424 ± 15
43	technetium	^{98}Tc	97.907	(428 ± 35)
44	ruthenium	Ru	101.07	(441 ± 35)
45	rhodium	Rh	102.9055	449 ± 20
46	palladium	Pd	106.42	470 ± 20
47	silver	Ag	107.868	470 ± 10
48	cadmium	Cd	112.41	469 ± 20
49	indium	In	114.82	488 ± 20
50	tin	Sn	118.69	488 ± 15
51	antimony	Sb	121.75	(487 ± 40)
52	tellurium	Te	127.60	(485 ± 40)
53	iodine	I	126.9045	(474 ± 40) gas (491 ± 40) condensed
54	xenon	Xe	131.29	482 ± 30 gas
55	cesium	Cs	132.9054	(488 ± 40)
56	barium	Ba	137.33	(491 ± 40)
57	lanthanum	La	138.9055	(501 ± 40)
58	cerium	Ce	140.12	(523 ± 40)
59	praseodymium	Pr	140.9077	(535 ± 45)
60	neodymium	Nd	144.24	(546 ± 45)
61	promethium	^{145}Pm	144.913	(560 ± 45)
62	samarium	Sm	150.36	(574 ± 45)
63	europium	Eu	151.96	(580 ± 45)
64	gadolinium	Gd	157.25	591 ± 50
65	terbium	Tb	158.9254	(614 ± 55)
66	dysprosium	Dy	162.50	(628 ± 55)
67	holmium	Ho	164.9304	(650 ± 60)
68	erbium	Er	167.26	(658 ± 60)
69	thulium	Tm	168.9342	(674 ± 60)

Z	Element	Symbol	A,[a] g/mol	I,[b] eV
70	ytterbium	Yb	173.04	(684 ± 65)
71	lutetium	Lu	174.967	(694 ± 65)
72	hafnium	Hf	178.49	(705 ± 65)
73	tantalum	Ta	180.9479	718 ± 30
74	tungsten	W	183.85	727 ± 30
75	rhenium	Re	186.207	(736 ± 70)
76	osmium	Os	190.2	(746 ± 70)
77	iridium	Ir	192.22	757 ± 30
78	platinum	Pt	195.08	790 ± 30
79	gold	Au	196.9665	790 ± 30
80	mercury	Hg	200.59	(800 ± 75)
81	thallium	Tℓ	204.383	(810 ± 75)
82	lead	Pb	207.2	823 ± 30
83	bismuth	Bi	208.9804	(823 ± 80)
84	polonium	^{209}Po	208.982	(830 ± 80)
85	astatine	^{210}At	209.987	(825 ± 80)
86	radon	^{222}Rn	222.018	(794 ± 80) gas
87	francium	^{223}Fr	223.020	(827 ± 80)
88	radium	Ra	226.0254	(826 ± 80)
89	actinium	Ac	227.0278	(841 ± 80)
90	thorium	Th	232.0381	(847 ± 80)
91	protactinium	Pa	231.0359	(878 ± 80)
92	uranium	U	238.0289	890 ± 30
93	neptunium	Np	237.0482	(902 ± 80)
94	plutonium	^{239}Pu	239.052	(921 ± 85)
95	americium	^{243}Am	243.061	(934 ± 85)
96	curium	^{247}Cm	247.070	(939 ± 85)
97	berkelium	^{247}Bk	247.070	(952 ± 85)
98	californium	^{251}Cf	251.080	(966 ± 90)
99	einsteinium	^{252}Es	252.083	(980 ± 90)
100	fermium	^{257}Fm	257.095	(994 ± 90)

[a] The atomic weights A are those recommended by the Commission on Atomic Weights of the International Union of Pure and Applied Chemistry (Holden [53]). The values are for naturally occuring isotopic mixtures, unless a particular isotope is indicated.

[b] Values in parentheses are estimated by interpolation of I/Z *vs.* Z, or by extrapolation for $Z > 92$.

Table 2. Mean excitation energies adopted in the present work for atomic constituents of compounds.

GASES

Constituent	I(eV)
H	19.2
C	70
N	82
O	97

LIQUIDS AND SOLIDS

Constituent	I(eV)
H	19.2
C	81
N	82
O	106
F	112
Cℓ	180
Others	1.13 x I, where I is the I-value for the element in the condensed phase given in Table 1.

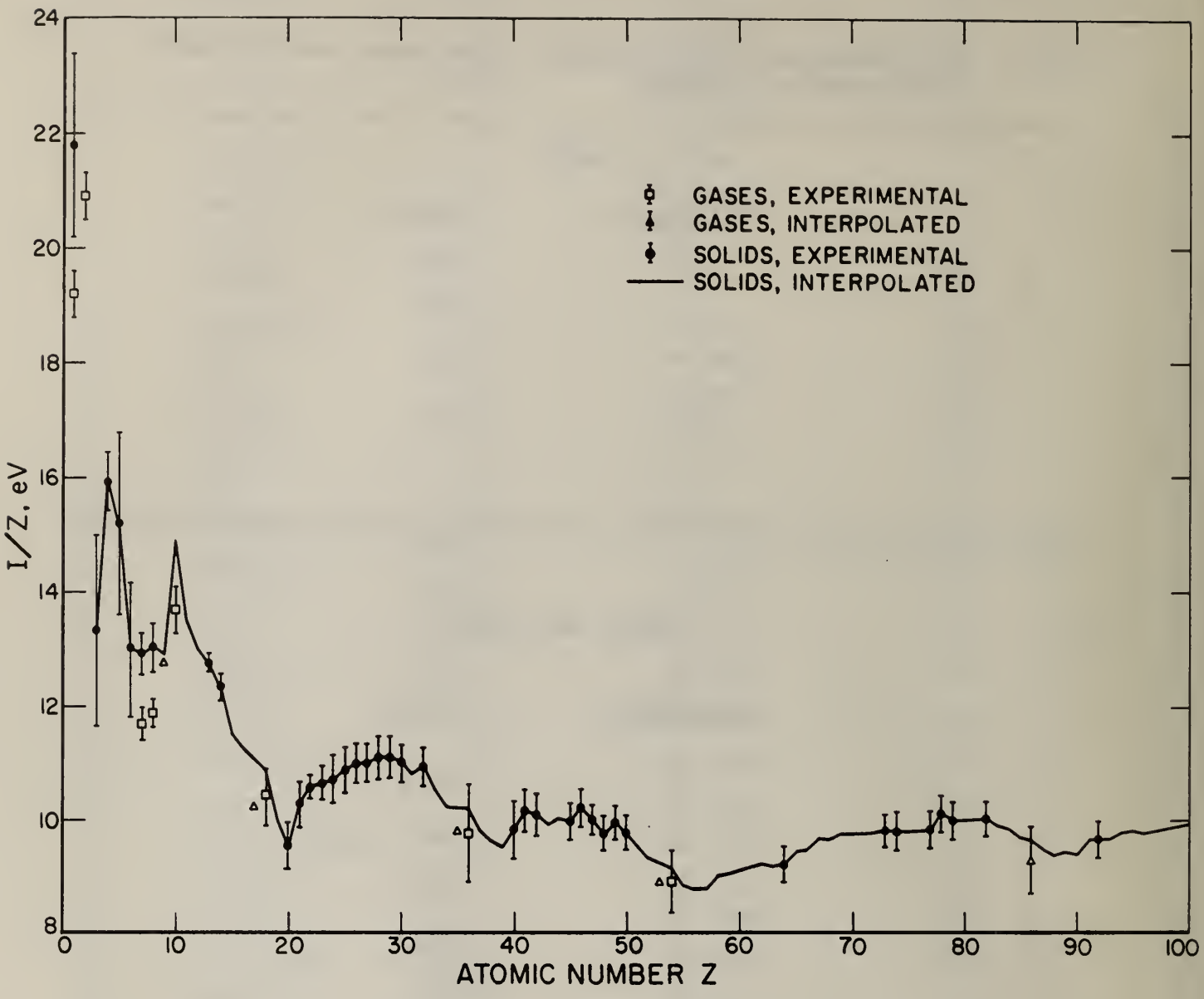

Fig. 1. Ratio of the mean excitation energy I to the atomic number Z for elements. Points indicated as experimental are the result of a critical analysis of experimental data; interpolated results are based in part on the theoretical results of Chu and Powers [15] for gases or of Ziegler [54] for solids.

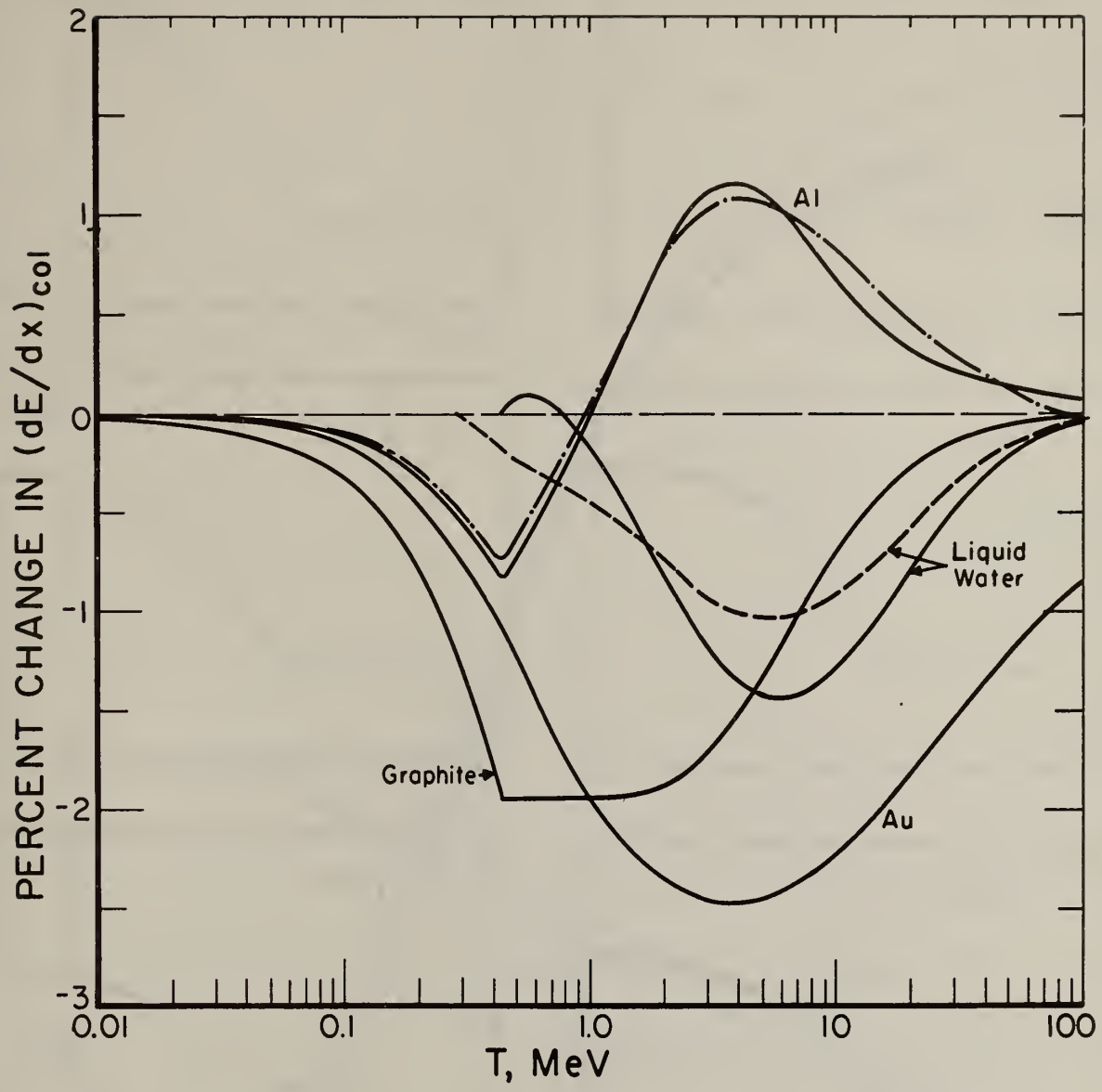

Fig. 2. Percent change in collision stopping power $\left(\frac{dE}{dx}\right)_{col}$ resulting from the use of the density-effect correction from a new, more accurate, numerical evaluation rather than that calculated according to the algorithm of Sternheimer and Peierls [10]. The solid curves, given as a function of electron kinetic energy T, are from the present work evaluated according to Sternheimer's [12] model; the broken curves were derived from experimental information on the dielectric-response function by Inokuti and Smith [13] for aluminum and by Ashley [14] for liquid water. The sharp corners in the curves are due to the approximate cut-off procedure in the Sternheimer-Peierls algorithm.

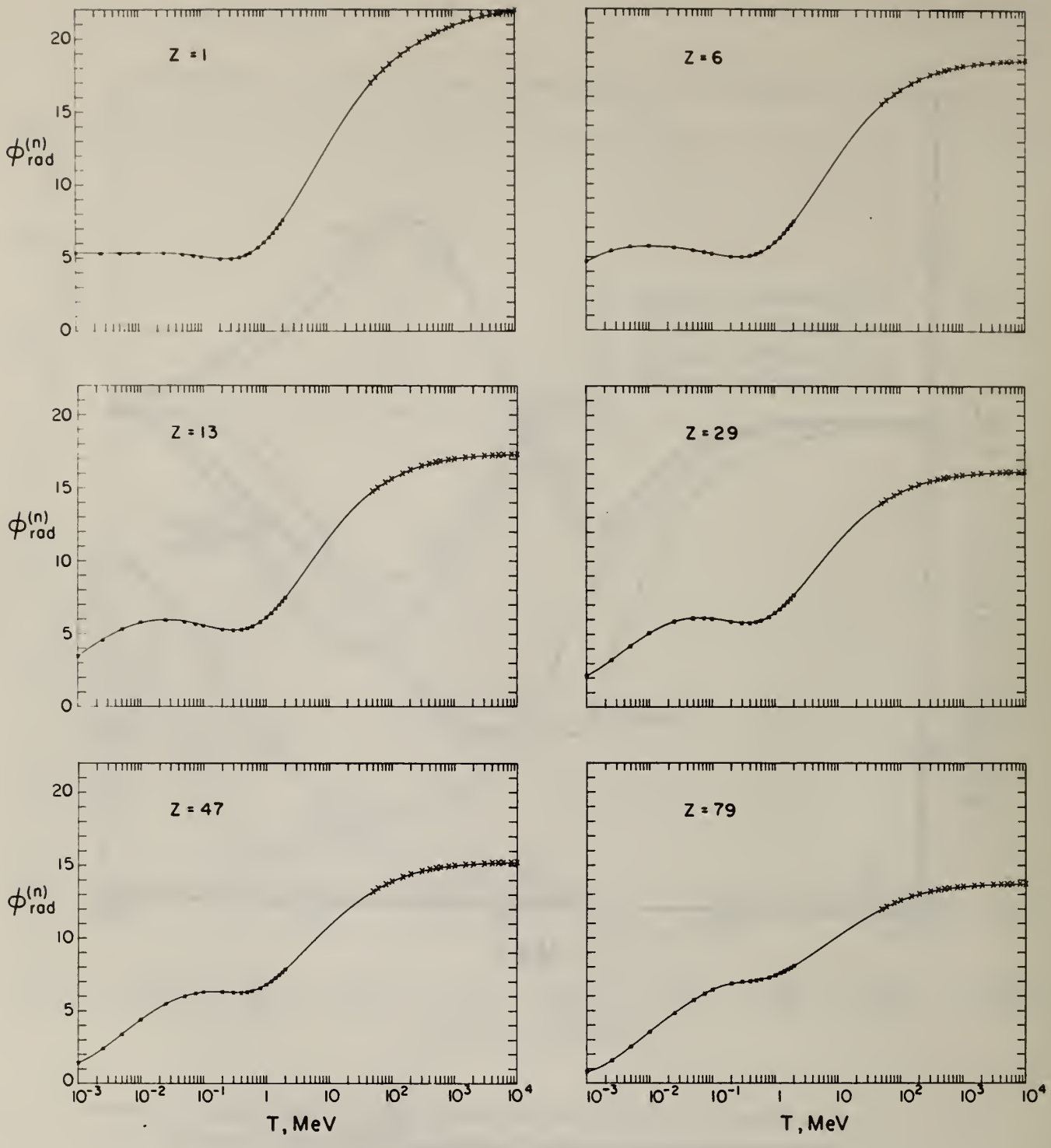

Fig. 3. Radiative energy-loss function $\phi^{(n)}_{rad}$ for bremsstrahlung in the field of the atomic nucleus. Points below 2 MeV are from the calculations of Pratt *et al.* [18]; points above 50 MeV were calculated using Bethe-Heitler theory with Hartree-Fock form-factor [55-56] screening corrections and the Coulomb correction of Davies, Bethe, Maximon, and Olsen [17]. Curves are from a least-squares fit to the theoretical points.

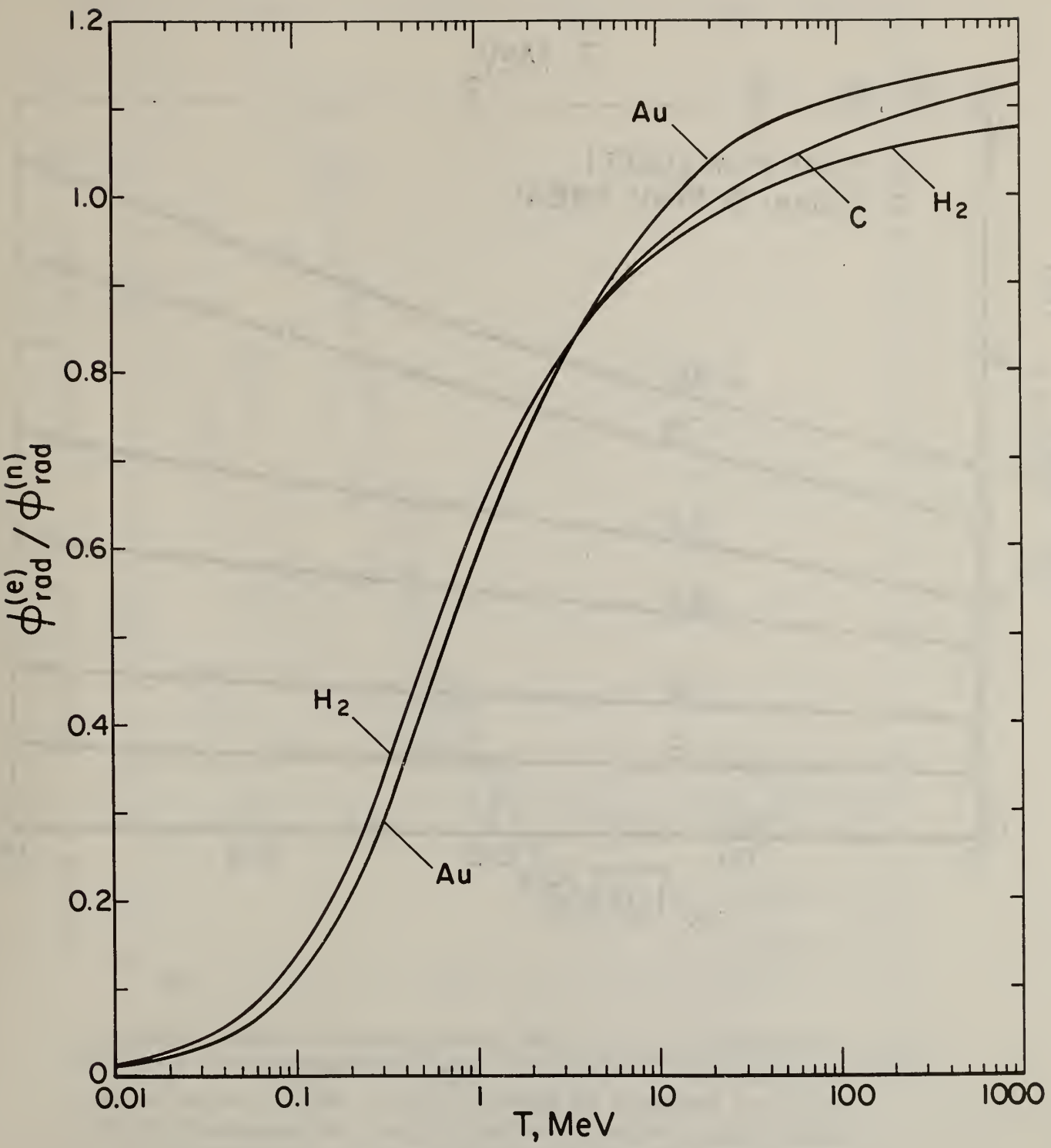

Fig. 4. Ratio of the radiative energy-loss functions $\phi^{(e)}_{rad}$ and $\phi^{(n)}_{rad}$ which represent the mean energy losses resulting from bremsstrahlung emission in the field of the atomic electrons, and the field of the atomic nucleus, respectively. The results for $\phi^{(e)}_{rad}$ are based on Haug's [20] theory of electron-electron bremsstrahlung with screening corrections evaluated according to Wheeler and Lamb [57] using Hartree-Fock incoherent scattering functions [55]. The total radiative stopping power is proportional to $Z^2\ \phi^{(n)}_{rad} + Z\ \phi^{(e)}_{rad}$.

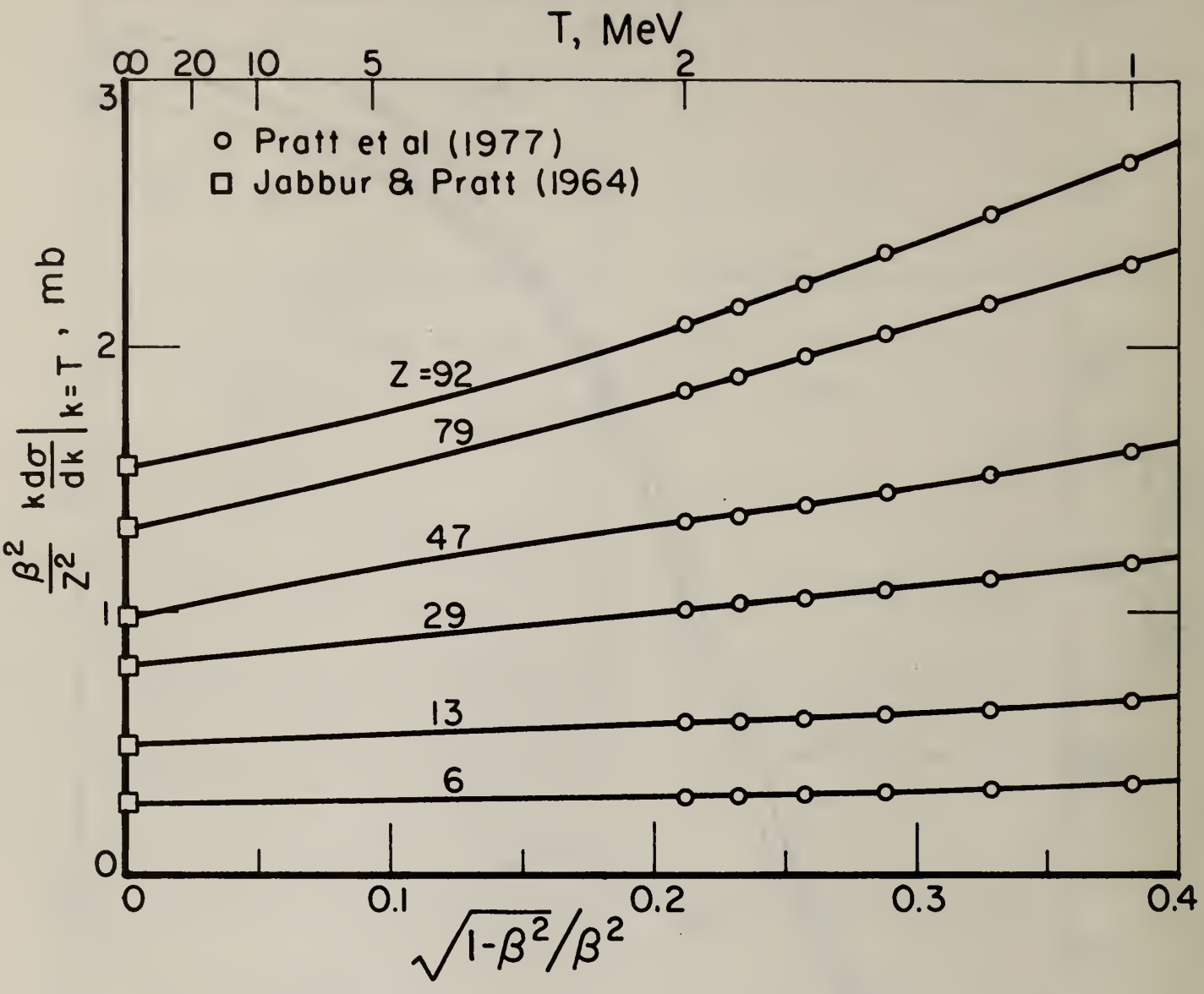

Fig. 5. High-frequency limit (tip) of the electron-nucleus differential bremsstrahlung cross section. The scaled tip value, $(\beta^2/Z^2)k(d\sigma/dk)$ for $k = T$, is plotted as a function of the variable $\sqrt{1-\beta^2}/\beta^2$, where β is the incident electron velocity divided by the speed of light. The corresponding initial electron kinetic energy is given on the upper scale. The squares are the results of the theory of Jabbur and Pratt [21] for $\beta = 1$; the circles below 2 MeV are from the data of Pratt *et al.* [18]. The curves, nearly straight lines when plotted in terms of these variables, are least-squares fits to the theoretical points.

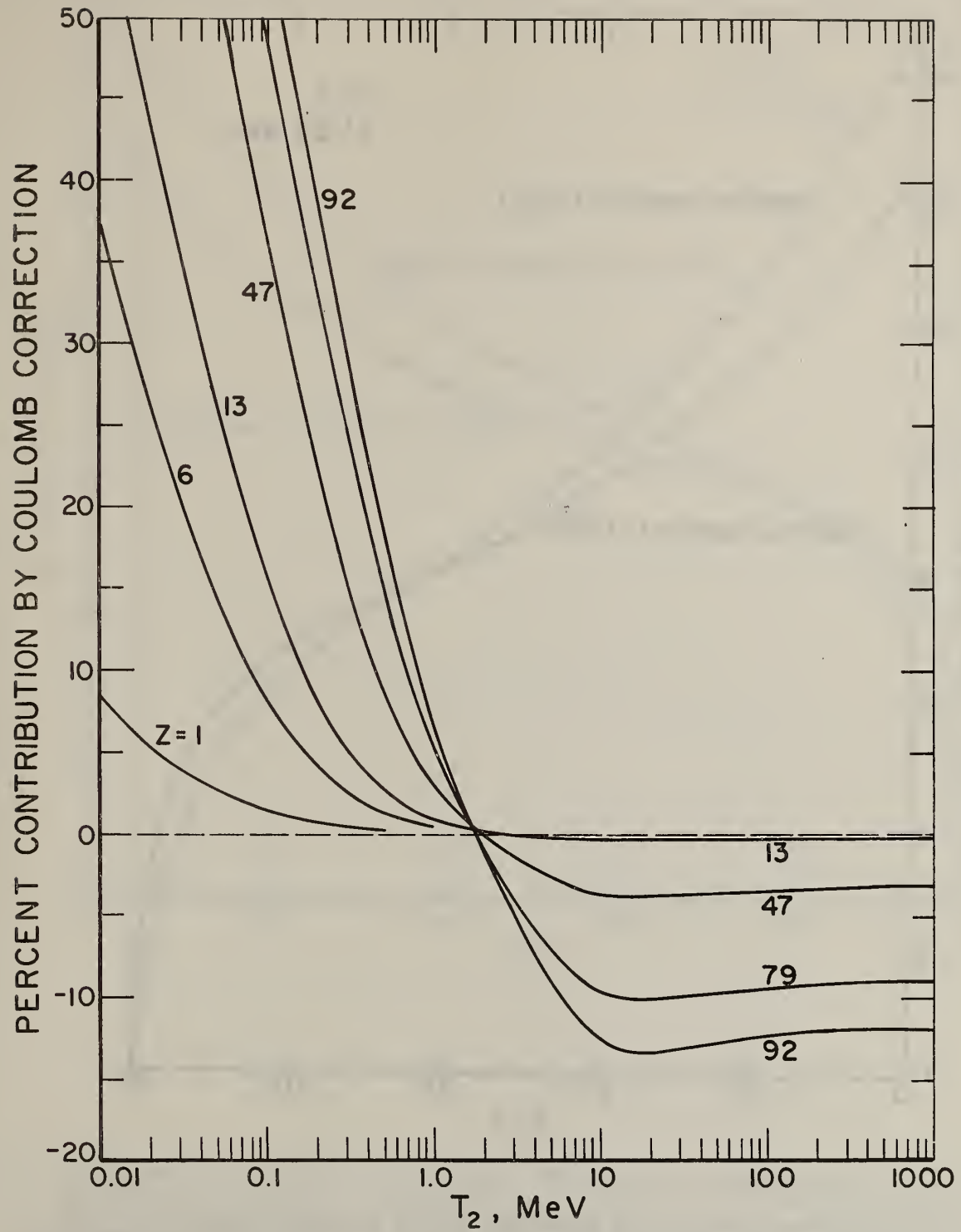

Fig. 6. Contribution of the Coulomb correction to the high-energy electron-nucleus bremsstrahlung cross section differential in emitted photon energy. The percent contribution to the final cross section is given as a function of the final kinetic energy T_2 of the electron after the emission of a bremsstrahlung photon. The results are nearly the same for all initial electron kinetic energies $\gtrsim$ 50 MeV.

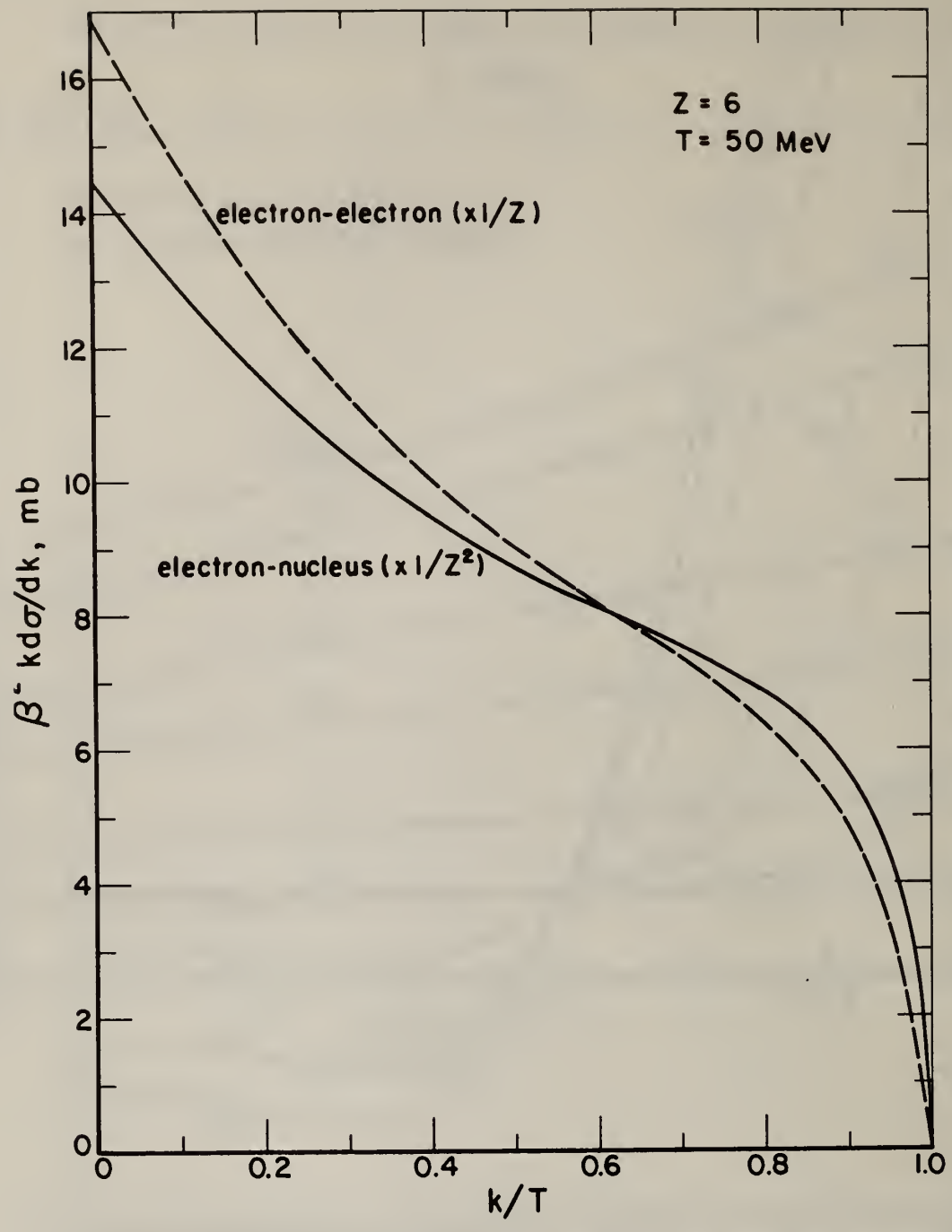

Fig. 7. Bremsstrahlung production cross section, differential in emitted photon energy. Shown is the scaled cross section $\beta^2 k(d\sigma/dk)$ *vs.* the ratio k/T of the emitted photon energy to the initial electron kinetic energy. The solid curve is the electron-nucleus cross section divided by Z^2, and the dashed curve is the electron-electron cross section divided by Z, where Z is the atomic number of the target.

a. Carbon ($Z = 6$), $T = 50$ MeV.

For $T = 50$ MeV, the electron-nucleus results are from a synthesis of Bethe-Heitler theory, screening corrections evaluated in the high-energy approximation using Hartree-Fock atomic form factors [55,56], and a Coulomb correction combining the theoretical results of Davies, Bethe, Maximon, and Olsen [17] and of Elwert [22], modified to go smoothly into the high-frequency limit given by the theory of Jabbur and Pratt [21]. The electron-electron results are from the theory of Haug [20], with screening corrections evaluated in the high-energy approximation using Hartree-Fock incoherent scattering factors [55].

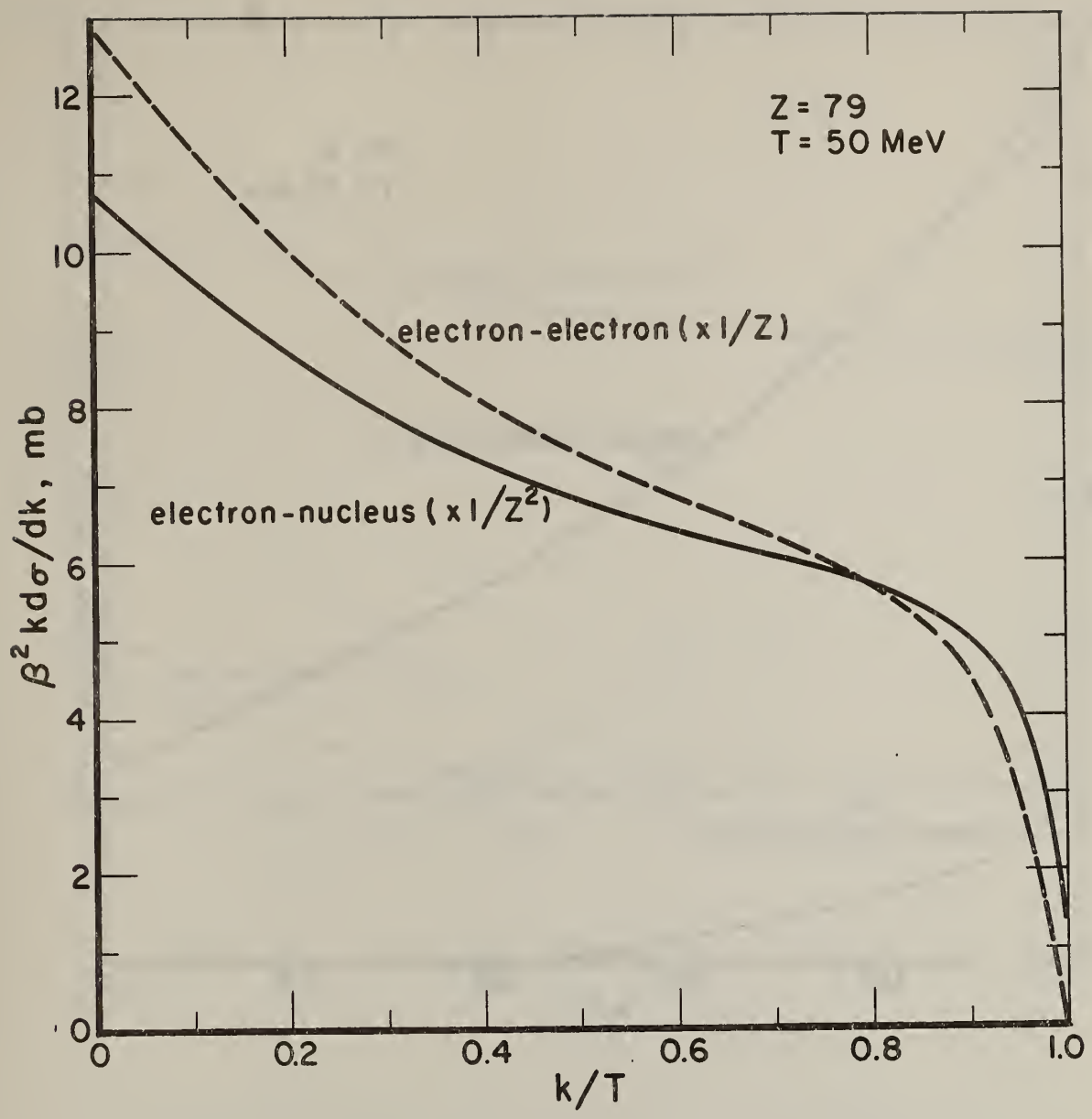

Fig. 7. Bremsstrahlung production cross section, differential in emitted photon energy. Shown is the scaled cross section $\beta^2\, k(d\sigma/dk)$ *vs.* the ratio k/T of the emitted photon energy to the initial electron kinetic energy. The solid curve is the electron-nucleus cross section divided by Z^2, and the dashed curve is the electron-electron cross section divided by Z, where Z is the atomic number of the target.

b. Gold ($Z = 79$), $T = 50$ MeV.

For $T = 50$ MeV, the electron-nucleus results are from a synthesis of Bethe-Heitler theory, screening corrections evaluated in the high-energy approximation using Hartree-Fock atomic form factors [55,56], and a Coulomb correction combining the theoretical results of Davies, Bethe, Maximon, and Olsen [17] and of Elwert [22], modified to go smoothly into the high-frequency limit given by the theory of Jabbur and Pratt [21]. The electron-electron results are from the theory of Haug [20], with screening corrections evaluated in the high-energy approximation using Hartree-Fock incoherent scattering factors [55].

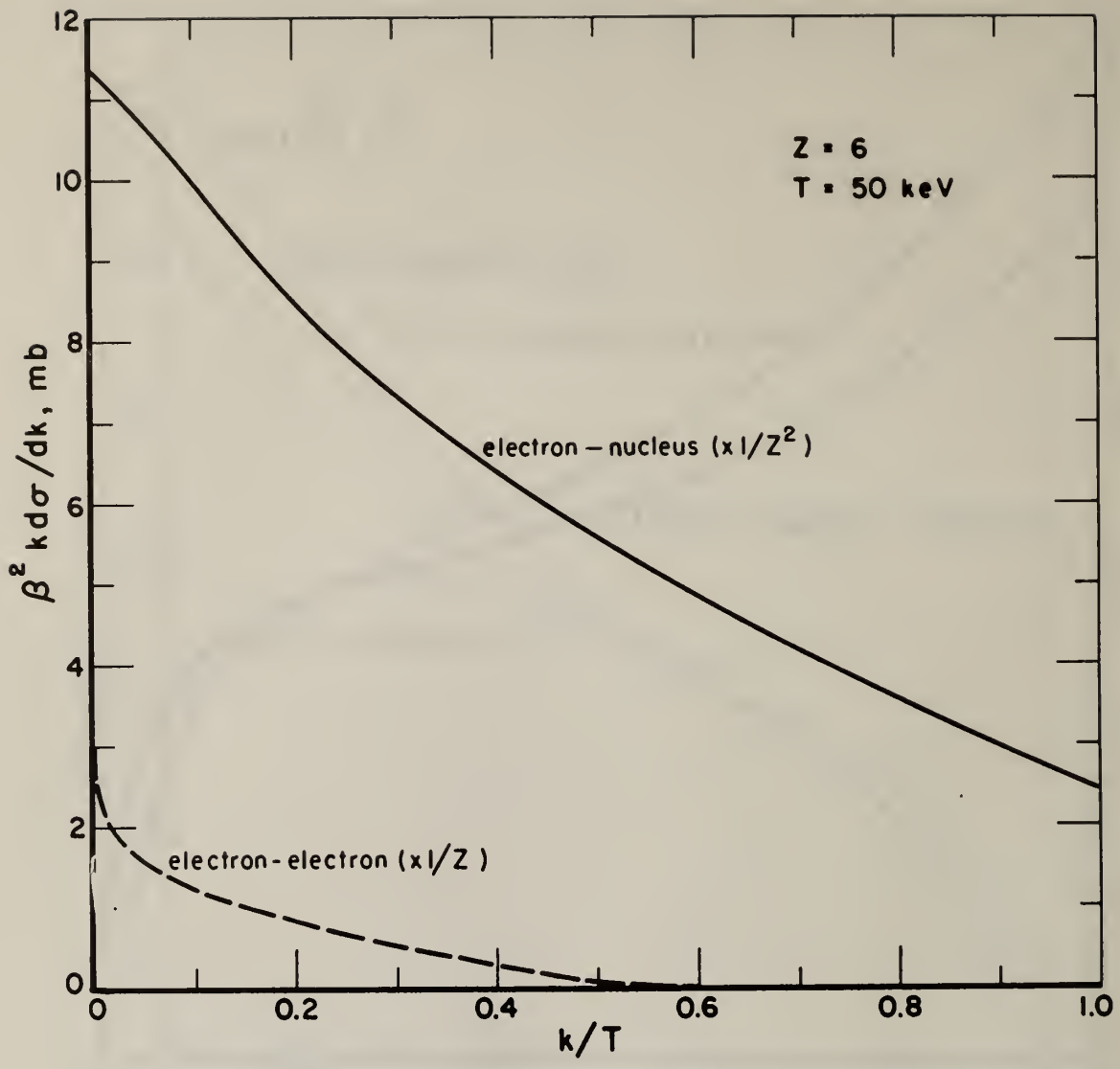

Fig. 7. Bremsstrahlung production cross section, differential in emitted photon energy. Shown is the scaled cross section $\beta^2\, k(d\sigma/dk)$ *vs.* the ratio k/T of the emitted photon energy to the initial electron kinetic energy. The solid curve is the electron-nucleus cross section divided by Z^2, and the dashed curve is the electron-electron cross section divided by Z, where Z is the atomic number of the target.

c. Carbon ($Z = 6$), $T = 50$ keV.

For $T = 50$ keV, the electron-nucleus results are from the calculations of Pratt *et al.* [18]. The electron-electron results are from the theory of Haug [20]; screening corrections which would somewhat modify the rather steep portion of the curves near $k = 0$ have been neglected.

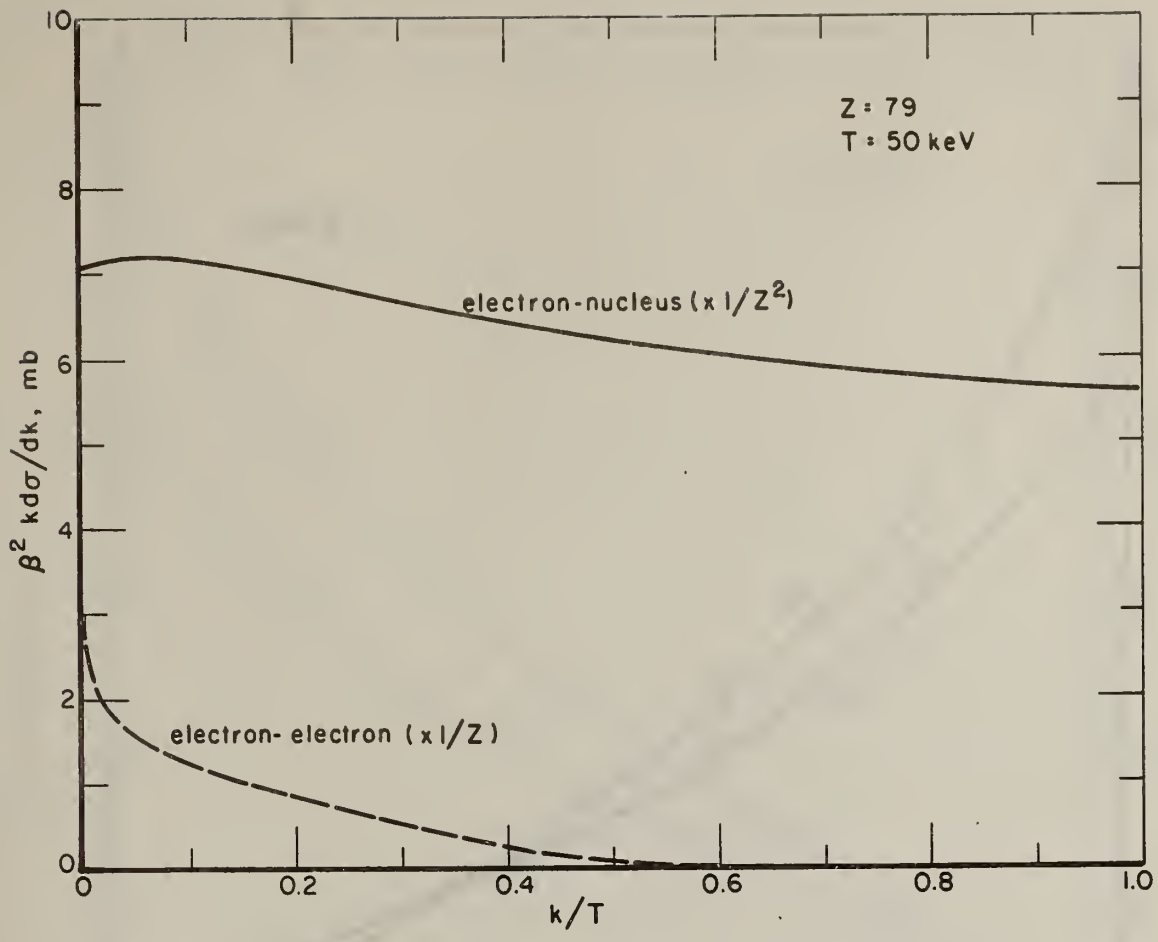

Fig. 7. Bremsstrahlung production cross section, differential in emitted photon energy. Shown is the scaled cross section $\beta^2\, k(d\sigma/dk)$ *vs.* the ratio k/T of the emitted photon energy to the initial electron kinetic energy. The solid curve is the electron-nucleus cross section divided by Z^2, and the dashed curve is the electron-electron cross section divided by Z, where Z is the atomic number of the target.

d. Gold ($Z = 79$), $T = 50$ keV.

For $T = 50$ keV, the electron-nucleus results are from the calculations of Pratt *et al.* [18]. The electron-electron results are from the theory of Haug [20]; screening corrections which would somewhat modify the rather steep portion of the curves near $k = 0$ have been neglected.

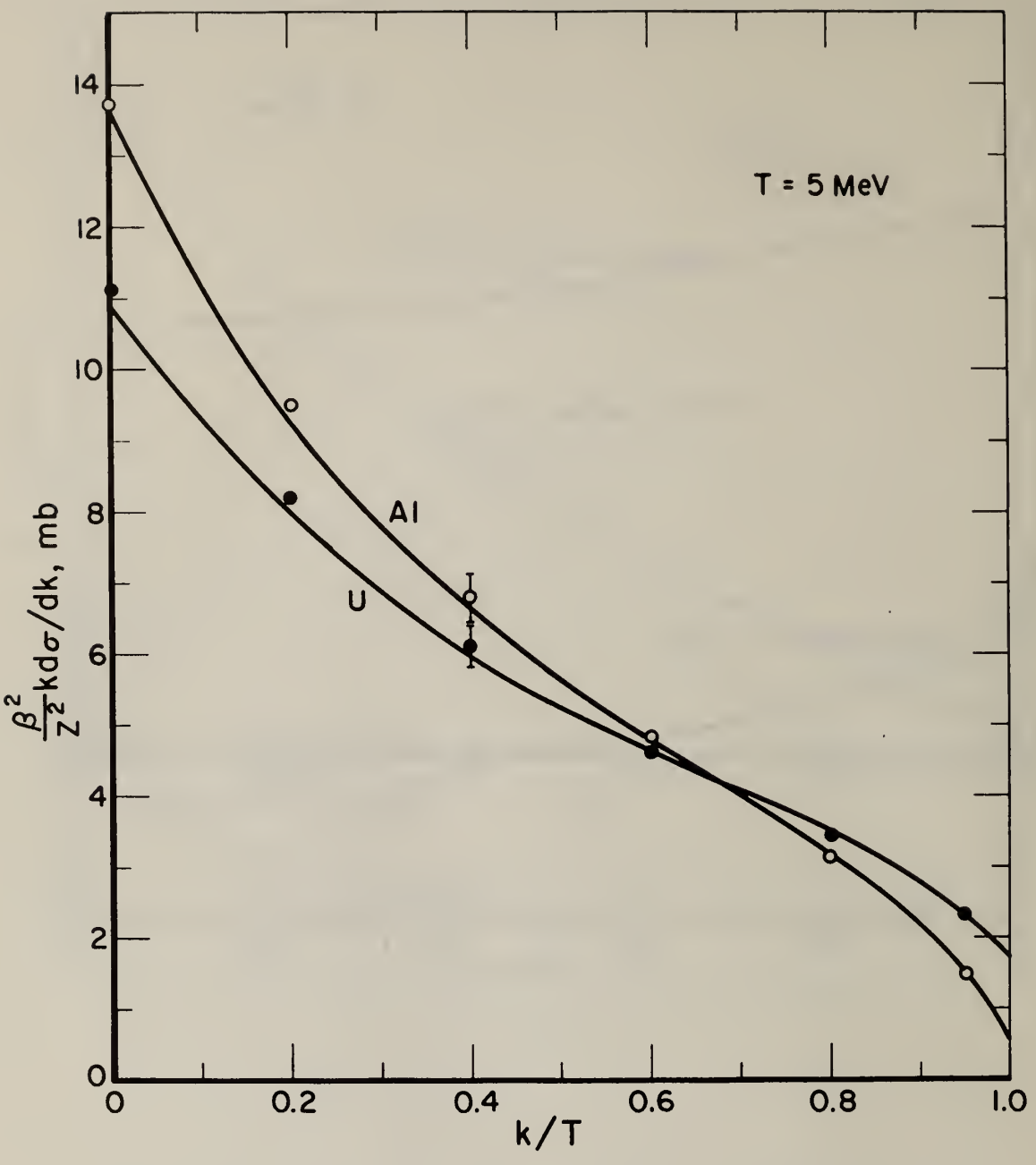

Fig. 8. Comparison of interpolated differential electron-nucleus bremsstrahlung cross sections with the results of exact calculations by Tseng and Pratt [23]. Shown is the scaled cross section $(\beta^2/Z^2)k(d\sigma/dk)$ plotted as a function of the ratio k/T, where β is the ratio of the initial electron velocity to the speed of light, Z is the atomic number of the target, k is the emitted photon energy, and T is the initial electron kinetic energy. The curves are from interpolation between the high-energy results ($T \geq 50$ MeV) and the results of Pratt *et al.* [18] ($T \leq 2$ MeV). The points are from the pilot calculations of Tseng and Pratt [23]; the error bars are drawn to indicate a ± 5% uncertainty.

a. Aℓ and U, T = 5 MeV.

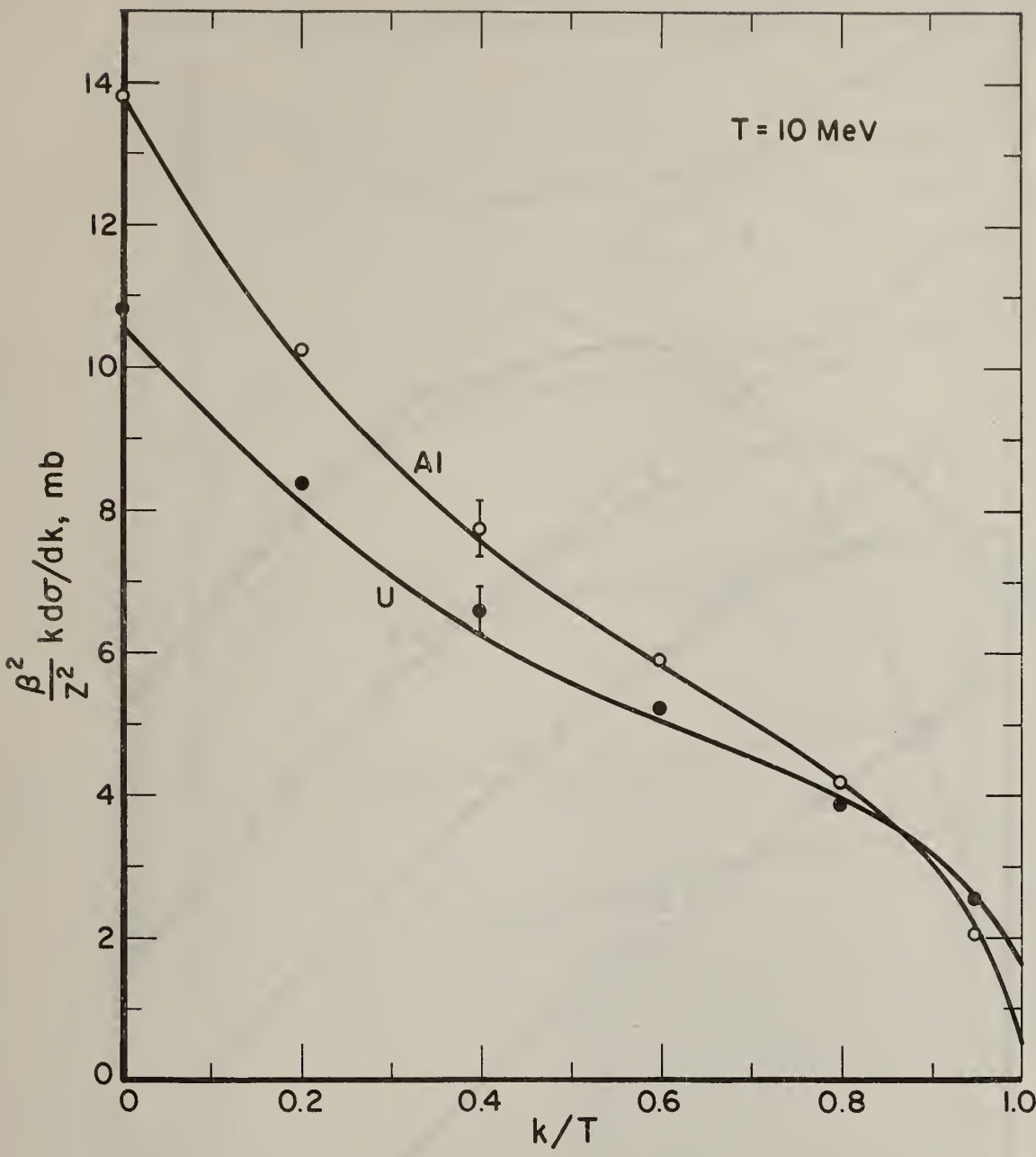

Fig. 8. Comparison of interpolated differential electron-nucleus bremsstrahlung cross sections with the results of exact calculations by Tseng and Pratt [23]. Shown is the scaled cross section $(\beta^2/Z^2)k(d\sigma/dk)$ plotted as a function of the ratio k/T, where β is the ratio of the initial electron velocity to the speed of light, Z is the atomic number of the target, k is the emitted photon energy, and T is the initial electron kinetic energy. The curves are from interpolation between the high-energy results ($T \geq 50$ MeV) and the results of Pratt *et al.* [18] ($T \leq 2$ MeV). The points are from the pilot calculations of Tseng and Pratt [23]; the error bars are drawn to indicate a ± 5% uncertainty.

b. Aℓ and U, T = 10 MeV.

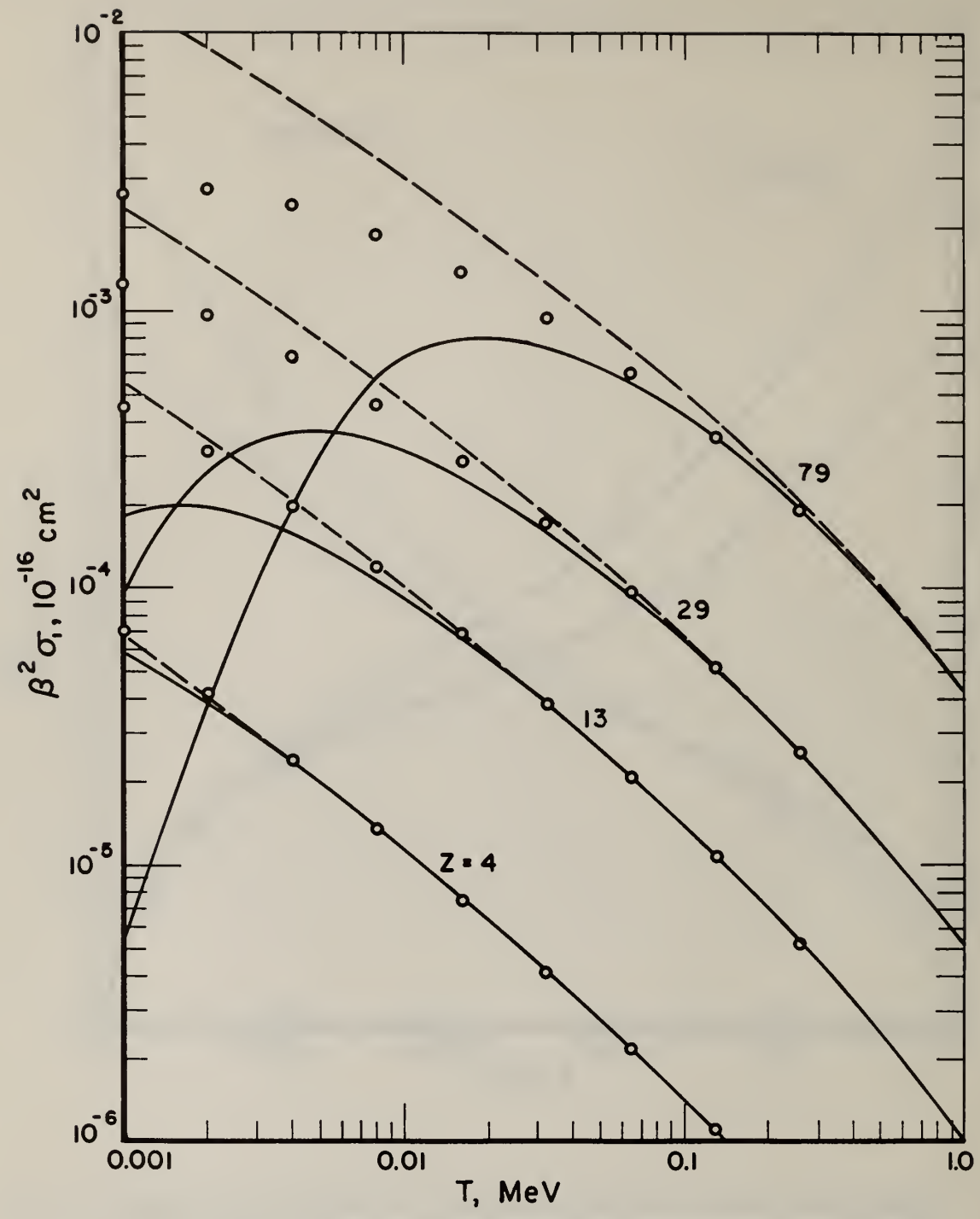

Fig. 9. Transport cross sections for elastic scattering, at electron energies below 1 MeV. The quantity given is $\beta^2\sigma_1(T)$, where β is the ratio of the electron velocity to the speed of light, and $\sigma_1(T) = 2\pi\int_0^{\pi} [d\sigma(\theta,T)/d\Omega](1 - \cos\theta)\sin\theta d\theta$. The curves are results based on the factorization of $d\sigma/d\Omega$ (Mott cross section x screening correction). The solid curves are for a screening correction calculated with a screening parameter according to Molière [26]. The dashed curves are with a screening correction in terms of a form factor, $(1 - F)^2$. The points are from the results of the phase-shift calculations of Riley *et al.* [28] for a static, screened Coulomb potential.

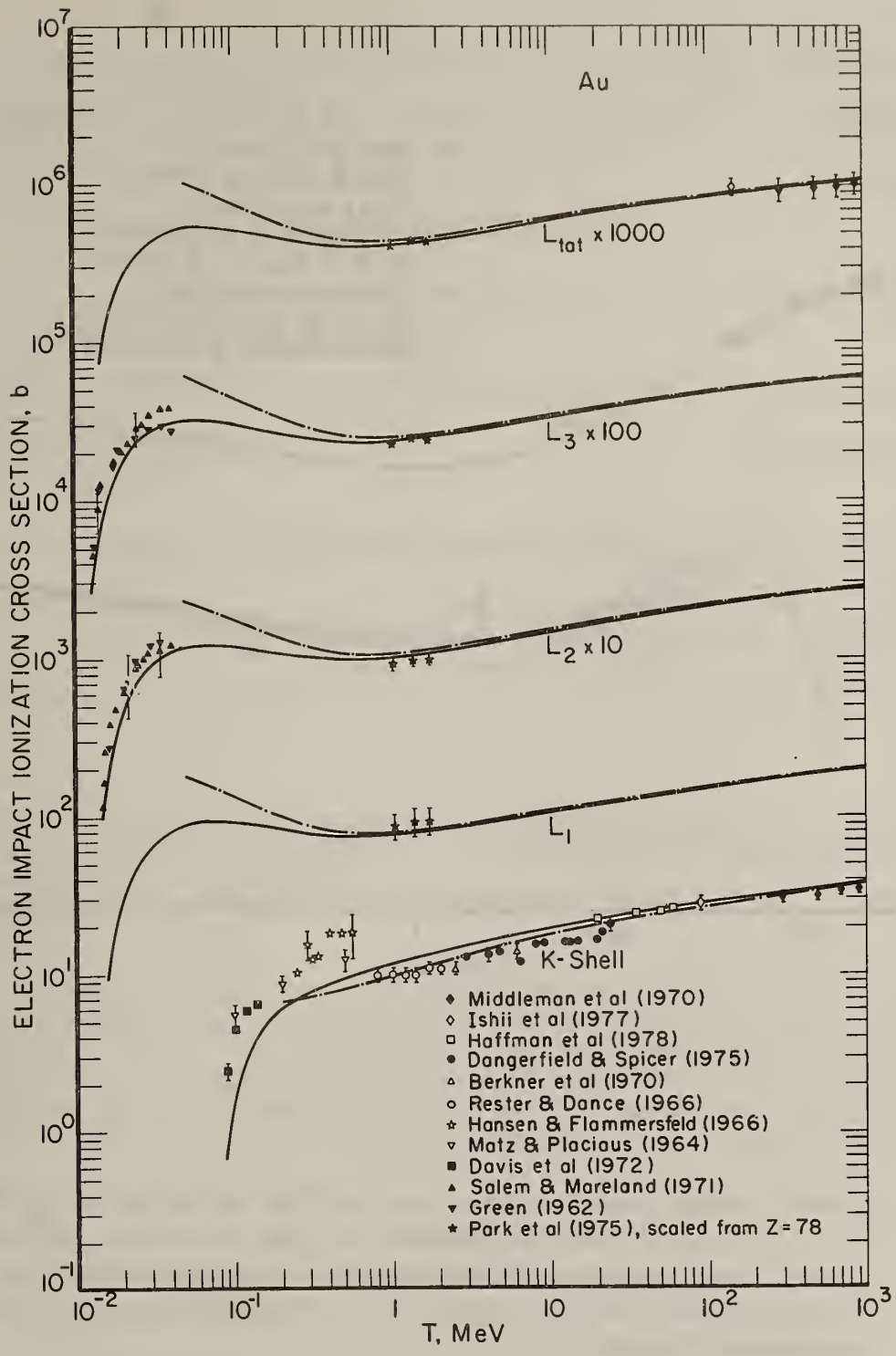

Fig. 10. Comparison of theoretical electron impact ionization cross sections for K and L shells in gold with experimental results. The solid curves are from our Weizsäcker-Williams calculations, and the broken curves are from Scofield's [32] Born-approximation calculations. The points are from various measurements [33-44].

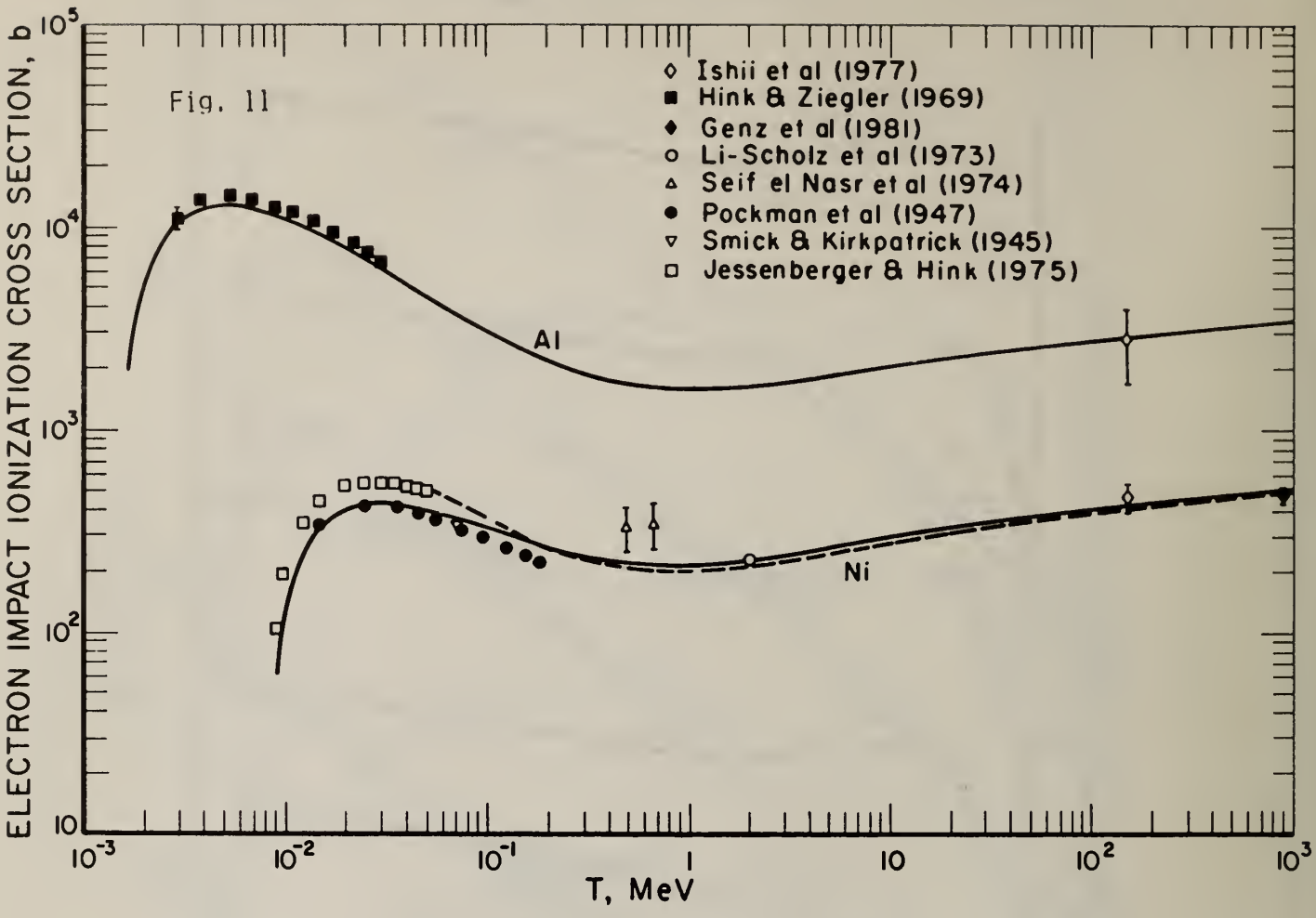

Fig. 11. K-shell electron impact ionization cross sections in aluminum and nickle. The solid curves are from our Weizsäcker-Williams calculations; the broken curve is from Scofield's [32] Born-approximation calculations (Scofield did not calculate the cross section for Aℓ). The points are from various measurements [34,45-51].

NBS-114A (REV. 2-8C)

U.S. DEPT. OF COMM. BIBLIOGRAPHIC DATA SHEET (See instructions)	1. PUBLICATION OR REPORT NO. NBSIR 82-2572	2. Performing Organ. Report No.	3. Publication Date September 1982

4. TITLE AND SUBTITLE

STATUS OF ELECTRON TRANSPORT CROSS SECTIONS

5. AUTHOR(S)

S. M. Seltzer and M. J. Berger

6. PERFORMING ORGANIZATION (If joint or other than NBS, see instructions)

NATIONAL BUREAU OF STANDARDS
DEPARTMENT OF COMMERCE
WASHINGTON, D.C. 20234

7. Contract/Grant No.

8. Type of Report & Period Covered

9. SPONSORING ORGANIZATION NAME AND COMPLETE ADDRESS (Street, City, State, ZIP)

Office of Naval Research
Arlington, Virginia 22217

Space Science Data Center
NASA Goddard Space Flight Center
Greenbelt, Maryland 20771

Office of Health and Environmental Research
Department of Energy
Washington, D.C. 20545

10. SUPPLEMENTARY NOTES

☐ Document describes a computer program; SF-185, FIPS Software Summary, is attached.

11. ABSTRACT (A 200-word or less factual summary of most significant information. If document includes a significant bibliography or literature survey, mention it here)

This report describes recent developments and improvements pertaining to cross sections for electron-photon transport calculations. The topics discussed include: (1) electron stopping power (mean excitation energies, density-effect correction); (2) bremsstrahlung production by electrons (radiative stopping power, spectrum of emitted photons); (3) elastic scattering of electrons by atoms; (4) electron-impact ionization of atoms.

12. KEY WORDS (Six to twelve entries; alphabetical order; capitalize only proper names; and separate key words by semicolons)

bremsstrahlung; cross sections; elastic scattering; electron-impact ionization; electrons; photons; stopping power; transport.

13. AVAILABILITY

☒ Unlimited
☒ For Official Distribution. Do Not Release to NTIS
☐ Order From Superintendent of Documents, U.S. Government Printing Office, Washington, D.C. 20402.
☒ Order From National Technical Information Service (NTIS), Springfield, VA. 22161

14. NO. OF PRINTED PAGES

30

15. Price

$7.50